Petroleum Science 23 (2026) 762–776

Contents lists available at ScienceDirect

Petroleum Science

journal homepage: www.keaipublishing.com/en/journals/petroleum-science

Original Paper

Numerical investigation of natural gas-enhanced autothermic pyrolysis for optimizing in-situ conversion in oil shale

Chao-Fan Zhu [a,b,c,d,e], Tan-En Jiang [a,b,c,d,e], Shan-Shan Yao [f], Jia-Zong Li [a,b,c,d,e], Rui Jia [a,b,c,d,e], Wei Guo [a,b,c,d,e,*]

[a] College of Construction Engineering, Jilin University, Changchun, 130026, Jilin, China
[b] State Key Laboratory of Deep Earth Exploration and Imaging, Changchun, 130026, Jilin, China
[c] National-Local Joint Engineering Laboratory of In-situ Conversion, Drilling and Exploitation Technology for Oil Shale, Changchun, 130021, Jilin, China
[d] Provincial and Ministerial Co-construction of Collaborative Innovation Center for Shale Oil & Gas Exploration and Development, Jilin University, Changchun, 130021, Jilin, China
[e] Key Lab of Ministry of Natural Resources for Drilling and Exploitation Technology in Complex Conditions, Jilin University, Changchun, 130021, Jilin, China
[f] Department of Civil and Environmental Engineering and School of Petroleum and Mining Engineering, Edmonton, Alberta, T6G 1H9, Canada

ARTICLE INFO

Article history:
Received 10 April 2025
Received in revised form
18 November 2025
Accepted 18 November 2025
Available online 22 November 2025

Edited by Jia-Jia Fei

Keywords:
Oil shale
Autothermic pyrolysis in-situ conversion process
Natural gas-assisted
Energy efficiency

ABSTRACT

The autothermic pyrolysis in-situ conversion process for oil shale (ATS) offers the advantages of low development costs and the capability to exploit deep oil shale resources. However, oil shale formations with low oil content encounter the challenge of insufficient heat-generating donors in the thermal cracking residue, making it difficult to sustain the autogenous thermal reaction through oxidative exotherm. In this study, we propose a natural gas-assisted autogenous thermal in-situ conversion technology (H-ATS) designed to develop low oil content shale, and we analyze its mechanism through numerical simulation across oil shales with varying oil contents. The results show that introducing 2.0% natural gas into the injected air successfully triggers the autogenous thermal reaction in low-oil-content shale, achieving an energy efficiency of 3.70. For medium oil content shale, a 2.0% natural gas addition, and for high oil content shale, a 4.0% addition, significantly reduces the gas compression energy required, enhancing energy efficiency to 8.11 and 13.04, respectively—representing improvements of 29.47% and 19.19% over the ATS process alone. This study evaluates the applicability of H-ATS technology across various oil shale formations, providing a new approach for the commercialization of in-situ conversion technology.

1. Introduction

Oil shale is an important source of fossil fuel with considerable global reserves. However, due to the generally low degree of thermal maturity in oil shale, much of the hydrocarbon exists as solid kerogen, rather than freely mobile oils (Zhao et al., 2018). With advancements in in-situ conversion process (ICP) technology, oil shale has the potential to become an essential alternative to conventional oil and gas sources (Dyni, 2003). A key technological development in this domain is the autothermic pyrolysis in-situ conversion process (ATS), which has emerged as a promising approach for resource extraction in oil shale formations (Kang et al., 2020; Sun et al., 2021; Xu, 2023). ATS technology primarily targets well-reformed oil shale formations by injecting oxygen-containing gases into preheated formations (Wang et al., 2022). Through this process, residual carbons—generated from the thermal cracking of kerogen—undergoes oxidation, releasing heat that convectively warms the surrounding formation (Guo et al., 2016). This, in turn, enables oil and gas products to flow into production wells via fractures.

Laboratory experiments by Sun et al. (2015b) demonstrated that injecting air at 300 and 25 °C could successfully initiate the ATS reaction in oil shale samples. Guo et al. (2020) further showed through elemental analysis that the oxidation of residual carbon generated most of the required heat. Since ATS requires minimal external heat or combustible materials, it remains a cost-effective extraction technique (Guo et al., 2022).

* Corresponding author.
E-mail address: guowei6981@jlu.edu.cn (W. Guo).
Peer review under the responsibility of China University of Petroleum (Beijing).

https://doi.org/10.1016/j.petsci.2025.11.035

In 2016, Jilin University initiated a field pilot of ATS in the Songliao Basin, China (Bai et al., 2017), with cumulative oil production reaching 1.68 tonnes over three months, thereby verifying ATS feasibility (Liang et al., 2021). However, in oil shale formations with low to medium oil content (<5.0%), residual carbon levels after kerogen thermal cracking are insufficient, resulting in low heat generation and impeding the initiation or continuation of ATS (Yang et al., 2023b). To address this limitation, supplemental heat is necessary to maintain autogenic thermal reactions. Mixing air with natural gas during injection introduces an oxidizing reaction that generates additional heat, presenting a viable solution for low- and medium-oil-content oil shale. Such formations, which account for over half of global oil shale resources, represent a substantial opportunity for low-cost, efficient development. The theoretical potential exists to resolve the heat deficiency in low- and medium-oil-content formations by injecting a small proportion of natural gas during ATS: the resultant oxidation can heat the formation and support continuous reaction. However, combining natural gas and air in high-temperature settings introduces risks of oil loss and safety concerns. Therefore, a numerical simulation is essential to evaluate the feasibility and safety of natural gas-assisted ATS before laboratory and field testing.

Numerical simulation technology offers a low-cost approach to exploring complex in-situ conversion processes without the limitations of time and physical constraints. For example, Fan and Durlofsky (2010) used the GPRS framework at Stanford University to study the in-situ upgrading process, revealing a strong correlation between oil and gas production performance and heating temperature. Shen (2009) simulated the Shell Electrically Heated Field Experiment (Wang et al., 2018a) in Colorado's Piceance Basin using CMG STARS, achieving a good fit with field experimental data. Bauman et al. (2009) estimated an ideal energy efficiency and carbon footprint of 3 GJ/GJ and 36 kg/bbl, respectively, using numerical simulation. Lee and Moridis (2016) examined the impacts of effective porosity, oil shale grade, and natural fracture spacing on productivity and selectivity. In our previous study (Guo et al., 2023a), we explored the effects of preheating temperature, oxygen content, and injection rate on recovery and energy efficiency using an updated ATS model.

This paper presents a natural gas-assisted autothermic pyrolysis in-situ conversion process (H-ATS), where an optimized blend of natural gas in the injected air provides external energy to support ATS. The objective is to ensure successful initiation and sustainment of autogenic thermal reactions, especially for low-oil-content oil shale. A numerical model of the H-ATS was established using a "one injection, six production well" configuration, based on the oil shale conditions in the Songliao Basin with varying oil contents. This study analyzes the physical evolution of the formation, the production process of oil and gas, and the energy efficiency under H-ATS conditions.

2. Materials and methodology

2.1. Oil shale samples

This study focuses on the oil shale in the Songliao Basin located in Northeastern China recognized as one of the world's largest Cretaceous lake basins (Li et al., 2022; Xia et al., 2010). The basin developed semi-deep to deep lacustrine shale sedimentary layers rich in organic matter (Zhao et al., 2023). The basin can be divided into six first-order structural units. The target strata selected in this study belong to the Nenjiang Formation Member I, composed of grayish-black shale and oil shale deposited in deep and semi-deep lacustrine environments. The upper part of this formation consists of Nenjiang Formation Member II gray mudstone, while the lower part comprises green shale and siltstone. The kerogen type is predominantly Type I–II$_1$, indicating high-quality source rock. Vitrinite reflectance measurements show that the shale in this formation is of low maturity (Fan, 2022; Sun et al., 2022; Wang, 2013). The formation's original effective porosity is 6.40%, with an initial water saturation of 100% (Li and Cai, 2023; Shakib et al., 2015; Zhang et al., 2022). The thermal conductivity and heat capacity of the shale are 1.84×10^5 J/(m·day·°C) and 6.5×10^6 J/(m^3·°C), respectively (Guo et al., 2023b). With an apparent vitrinite reflectance (R_o) value of 0.5, the organic matter maturity is classified as low-maturity (early oil window), favoring the generation of oil-prone hydrocarbons. Mineralogical compositions are dominated by quartz (54%), followed by illite (20%) and calcite (6%). These mineral assemblages enhance organic matter preservation but may impose constraints on reservoir porosity and in-situ conversion processes due to their diagenetic stability and potential cementation effects (He et al., 2021; Tong et al., 2011; Wang et al., 2019; Zhu et al., 2022). Additional specific parameters of the oil shale are provided in Tables 1 and 2.

2.2. Numerical model

In this study, CMG STARSTM was used to simulate the H-ATS process in oil shale. As shown in Fig. 1, an inverse seven-spot well pattern was designed. To reduce computational demands, only one-sixth of the well pattern layout was modeled, incorporating one injection well and two production wells, based on symmetry principles. The well spacing is 50 m, with a control area of 1082.54 m^2 for the inverse seven-spot pattern. Heat loss at the top and bottom of the formation is neglected, as it is closely related to formation thickness, which is not a primary factor in this study. Fracturing technology is essential for H-ATS in tight sandstone formations; therefore, a dual-porosity model was applied to represent the fracture and matrix system. According to descriptions of the oil shale reservoir in the Songliao Basin, the shale formation permeability typically ranges from 10^{-5} to 10^{-1} mD, with a wide distribution in hydraulic fracture permeability (Dong et al., 2018; Wang et al., 2020). Consequently, matrix and fracture permeabilities were assumed to be 0.001 and 100 mD, respectively, for this model. The geological model was discretized into a 0.5 m × 0.5 m × 0.5 m grid using finite-difference discretization in a standard rectangular coordinate system (Fig. 1).

The optimal injection-production parameters for ATS were investigated in our previous study (Guo et al., 2023a). Based on those findings, the injection and production pressures were set to 10 MPa and 200 kPa, respectively. Gas injection was conducted in two stages. In the first stage, nitrogen gas heated to 500 °C was injected for three months to elevate the temperature near the injection well to the H-ATS trigger point. In the second stage, the injection gas was switched to a mixture of room temperature

Table 1
Physical characterization parameters of shales (He et al., 2021; Tong et al., 2011; Wang et al., 2019; Zhu et al., 2022).

Name	Assignment
Initial formation pressure, kPa	6500
Initial formation temperature, °C	35
Initial permeability, mD	0.05
Original porosity for matrix, %	6.4
Specific heat capacity, J/(m^3·°C)	6.5×10^6
Rock thermal conductivity, J/(m·day·°C)	1.84×10^5
The density of rock matrix, kg/m^3	2400
Initial water saturation in matrix, %	100
Apparent vitrinite reflectance R_o	0.5
Density of matrix, kg/m^3	1920

Table 2
Organic elemental analysis and mineral composition of the shale (Zhu et al., 2022).

Organic elemental analysis, %					Mineral composition, %							
C	H	O	N	S	Quartz	Alkali feldspar	Plagioclase	Calcite	Pyrite	Pyrite	Kaolinite	Chlorite
72.38	9.72	10.92	4.07	3.91	54	4	7	6	3	20	2	4

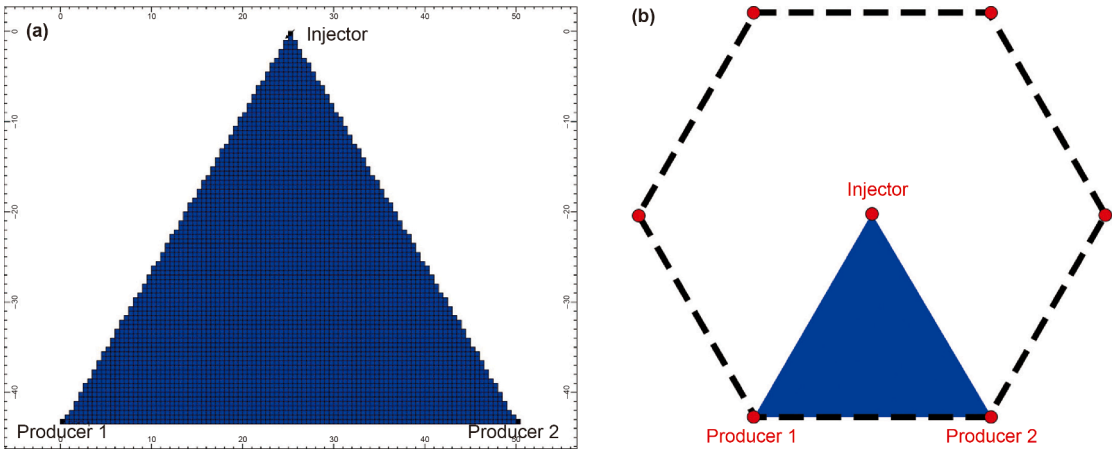

Fig. 1. Geologic model: (**a**) grid division; (**b**) well deployment method.

(20 °C) air and natural gas. This study examines nine cases with varying natural gas ratios across three different oil content shale formations.

2.3. Reaction model

The reaction model and kinetic parameters are essential prerequisites for conducting ATS numerical simulations, as they describe the chemical reaction processes and reaction rates of organic matter during heating (Yang et al., 2023a). The organic matter involved in H-ATS includes kerogen ($CH_{1.45}O_{0.04}N_{0.02}S_{0.01}$), natural gas ($C_{3.16}H_{8.33}$), heavy oil ($C_{27.17}H_{56.34}$), light oil ($C_{15.26}H_{32.52}$), prechar, and carbon (C). Additionally, O_2, H_2O, CO, and CO_2 are involved in the H-ATS process. The chemical reaction model for organic matter is presented in Table 3 (Braun and Burnham, 1992; Fowler and Vinegar, 2009; Guo et al., 2023a; He et al., 2019; Khakimova et al., 2019; Pei et al., 2018; Sun et al., 2015a). During H-ATS, it is assumed that two pyrolysis reactions and six oxidation reactions occur in the shale formation. As the temperature rises, kerogen first decomposes into natural gas, heavy oil, light oil, and prechar. When temperatures exceed 500 °C, kerogen further decomposes into natural gas and carbon. Besides the pyrolysis reactions, all organic compounds undergo oxidation, resulting in the formation of CO_2, CO, and H_2O in the high-temperature, oxygen-rich environment.

Studies on the interactions between water and organic matter have demonstrated that water plays both chemical and physical roles in the processes of oil generation and migration (Lewan, 1997). Hydrogenation reactions involving H_2O and H_2 significantly influence hydrocarbon gas formation and C/H isotope fractionation (He et al., 2025). In this study, prolonged injection of large volumes of air or air mixed with natural gas during the reaction process was primarily driven by the consideration of oxidation reactions of kerogen, precursor coke, and organic compounds with oxygen. Other reactions were deemed to have minimal impact on experimental outcomes and were therefore excluded from consideration, as existing models face challenges in accurately simulating these processes. Consequently, secondary cracking of oil and reactions between water and organic matter were not incorporated into the present analysis.

Based on the kinetic parameters (frequency factors, activation energies, and reaction enthalpies) for cracking reactions 1–2 provided by Braun and Burnham, these values have been applied in pilot-scale simulations at the Colorado Green River oil shale site (Braun and Burnham, 1992; Lee et al., 2018). Given the similarity in kerogen types (Type I-II) and depositional environments

Table 3
Chemical reaction model of the organic matter (Braun and Burnham, 1992; Fowler and Vinegar, 2009; Guo et al., 2023a; He et al., 2019; Khakimova et al., 2019; Pei et al., 2018; Sun et al., 2015a).

Number	Description	Reaction	Frequency factor, s^{-1}	Activation energy, kJ/mol	Reactionenthalpy, kJ/mol
1	Kerogen pyrolysis	$CH_{1.45}O_{0.04}N_{0.02}S_{0.01} = 0.0071C_{3.16}H_{8.33} + 0.0097C_{15.26}H_{32.52} + 0.0108C_{27.17}H_{56.34} + 0.6411$Prechar	3.0×10^{13}	213.50	−4.20
2	Prechar pyrolysis	Prechar $= 0.01718C_{3.16}H_{8.33} + 0.9902$C	1.0×10^{13}	226.09	−46.50
3	Kerogen oxidation	$CH_{1.45}O_{0.04}N_{0.02}S_{0.01} + 0.1052O_2 = 1.4225$Prechar	6.47×10^{4}	64.32	27.89
4	Prechar oxidation	Prechar $+ 1.1723O_2 = 0.5750H_2O + 0.78152CO_2 + 0.19538$CO	6.02×10^{8}	226.09	−46.50
5	Natural gas oxidation	$C_{3.16}H_{8.33} + 4.9296O_2 = 4.164H_2O + 2.5312CO_2 + 0.6328$CO	2.61×10^{5}	72.68	1758.46
6	Residual carbon oxidation	$C + 0.9O_2 = 0.8CO_2 + 0.2$CO	6.02×10^{8}	133.91	315.80
7	Heavy oil oxidation	$C_{27.17}H_{56.34} + 38.5359O_2 = 28.164H_2O + 21.7368CO_2 + 5.4342$CO	2.57×10^{7}	118.44	13735.40
8	Light oil oxidation	$C_{15.26}H_{32.52} + 21.864O_2 = 16.26H_2O + 12.208CO_2 + 3.052$CO	2.61×10^{5}	72.68	7794.69

(lacustrine shale formations) between the Songliao Basin and Green River oil shales, the kinetic parameters from the latter were adopted for the Songliao Basin's oil shale systems (Fowler and Vinegar, 2009; Pei et al., 2018). For formations with varying oil saturations, the reaction equations and activation energies remain consistent across different oil saturation levels, with distinctions arising solely from differences in initial kerogen concentrations. Consequently, the reaction equations presented in the table demonstrate robust applicability to oil shale formations in the Songliao Basin across diverse oil saturation conditions. The reaction kinetics, including the frequency factor, activation energy, and reaction enthalpy, describe the rate of these reactions and the heat changes across different temperatures.

In CMG, the kerogen concentration in shale pores determines the kerogen available for pyrolysis. Consequently, both the pyrolysis reaction model and kerogen concentration dictate the oil content of the shale. To establish the relationship between oil content and kerogen concentration, a grid unit with varying kerogen concentrations was configured. The Fischer assay analysis process (He et al., 2019; Zhu et al., 2022) was then replicated by gradually heating the grid unit to 520 °C in a nitrogen atmosphere. Using Eq. (1), the mass rate of oil production from the grid unit was calculated to determine the shale's oil content.

$$T_f = \frac{m_a}{m} \times 100\% \tag{1}$$

where T_f is the oil content of the shale; m_a is the mass of oil production, kg; m is the mass of the simulated formation grid unit, kg. Fig. 2 shows the relationship between the oil content and total organic carbon (TOC). The kerogen concentration increased from 35,255 to 59,383 mol/g when the oil content of shale rose from 3.0% to 10.0%. However, the kerogen concentration is not linear with the oil content of shale but a parabola. In this study, the low (3.0%), medium (5.0%), and high (10.0%) oil content shale formations in Songliao Basin are chosen to study the applicability of H-ATS in different shale formations. The kerogen concentrations of the three formations are 35,255, 46,312, and 59,384 mol/g, respectively. The oil content exhibits a significant positive correlation with TOC. As the oil content increases from 3% to 10%, the TOC value rises correspondingly from 3.11% to 19.12%, demonstrating concurrent increases between the two parameters. Notably, the magnitude of TOC enhancement is significantly greater than that of oil content, particularly in higher oil content ranges.

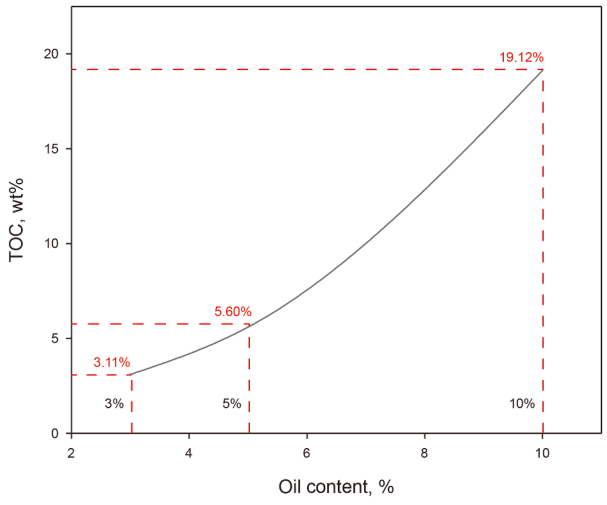

Fig. 2. Relationship between the oil content and total organic carbon.

2.4. Comparison model groups

To investigate the effectiveness of H-ATS development in formations with varying oil content, this study analyzed the impact of natural gas assistance on the autogenous thermal in-situ conversion of oil shale with different oil content with finding the key indicators such as oil and gas production and energy efficiency. Three sets of control models were created, each varying in the proportion of injected natural gas, to assess the applicability of H-ATS across formations with low, medium, and high oil content.

For low oil content formations, the models included: 100% air (L1), 98.0% air + 2.0% natural gas (L2), and 96.0% air + 4.0% natural gas (L3). For medium oil content formations, the models included: 100% air (M1), 98.0% air + 2.0% natural gas (M2), and 96.0% air + 4.0% natural gas (M3). For high oil content formations, the models included: 100% air (H1), 98.0% air + 2.0% natural gas (H2), and 96.0% air + 4.0% natural gas (H3). The specific oil content of each model and the injection-production parameters are detailed in Table 4.

2.5. Energy efficiency

Energy efficiency is a key comprehensive index representing the ratio of energy output to input during the H-ATS process. The energy conversion in H-ATS is divided into three components: (1) the compression energy required by the compressor to isothermally compress atmospheric gas into high-pressure gas, (2) the thermal energy used in injecting high-temperature nitrogen during the preheating stage, and (3) the chemical energy contained in the injected natural gas mixture and the produced hydrocarbons. The injected gas is assumed to be an ideal gas. Therefore, the power consumed by the compressor during isothermal compression can be calculated by Eq. (2):

$$N_c = 10^3 \times p_{sc} q \ln\frac{p_{in}}{p_{sc}} \tag{2}$$

where N_c is the compression energy power of injected gas, kJ/day; p_{sc} and p_{in} are the atmospheric pressure and injection pressure, MPa, respectively; q is the gas flow rate of the injection well, m^3/day. Because the main body of the injection gas and production gas are similar (the air proportion exceeds 95%), the effect of gas composition on the specific thermal capacity of the gas during the H-ATS can be neglected. The thermal energy of the injected and the product gas can be calculated using Eq. (3).

$$N_h = cq\rho\Delta t \tag{3}$$

where, N_h is the thermal energy of the gas, kJ/day; c is the specific thermal capacity of gas, kJ/(kg·°C); Δt is the temperature change of gas, °C; ρ is the density of the gas, kg/m^3. Considering that the chemical energy carried by the injected mixed gas primarily originates from the reinjected produced natural gas, we combine the injected air with the produced gas chemical energy in the discussion. The specific formula for energy efficiency is:

$$f_t = \frac{N_h^{out} + N_{og}}{N_h^{in} + N_c + N_g^{in}} \tag{4}$$

where f_t is the total energy efficiency; N_h^{out} is the thermal energy of the gas injected during the preheating stage, kJ; N_{og} is the calorific value of the produced hydrocarbons (oil and natural gas), kJ; N_h^{in} is

Table 4
Injection-production parameter for H-ATS model.

No.	Oil content, %	Natural gas ratio, %	Preheating temperature, °C	Preheating time, day
L1	3.0	0	500	90
L2		2.0		
L3		4.0		
M1	5.0	0		
M2		2.0		
M3		4.0		
H1	10.0	0		
H2		2.0		
H3		4.0		

the thermal energy carried by the gas, kJ; N_g^{in} is the calorific value of the injected natural gas, kJ. According to previous research (Wang et al., 2018b), the calorific values of oil and natural gas during the H-ATS are assumed to be 40.0×10^6 and 35.6×10^3 J/m^3. Therefore, the change in energy efficiency with time during H-ATS is obtained by Eqs. ((2)–(4)), and the end time of H-ATS should be at the peak of energy efficiency.

3. Results and discussion

The developed mathematical model was applied to investigate hydrocarbons (oil and gas) production, energy efficiency, temperature distribution, and kerogen evolution at key time points across shale formations of varying oil content and natural gas ratios. This analysis provides insights into the mechanisms that enhance energy efficiency and assesses the applicability of H-ATS in oil shale formations with different oil content levels.

3.1. Low oil content formation

To investigate the H-ATS process in low oil content shale formations, 100% air (L1), 98.0% air + 2.0% natural gas (L2), and 96.0% air + 4.0% natural gas (L3) were injected into a shale formation with an oil content of 2.9%. In this setup, L1 (100% air) serves as the baseline, representing the conventional ATS process in low oil content oil shale. Comparisons with L2 and L3 provide insights into the reaction efficiency of H-ATS for low oil content formations.

The relationships between oil and gas production over time for different natural gas ratios are shown in Fig. 3, while Fig. 4 illustrates the changes in energy efficiency over time. Fig. 5 presents a cloud diagram showing the distribution of kerogen and prechar, and Fig. 6 shows the temperature distribution within the formation. The specific analysis for each result is discussed below.

3.1.1. Hydrocarbon production

Hydrocarbon production from low oil-content oil shale using autogenous thermal in-situ extraction is shown in Fig. 3, based on the geological model developed (1/6 inverse seven-spot well network, stratum thickness of 0.5 m). This setup is consistent across the hydrocarbon output models used in this study. When injecting 100% air (L1), natural gas and oil production are 691.50 and 0.06 m^3, respectively. The natural gas production shows a brief increase following the preheating stage before leveling off, while oil production remains minimal, showing a significant difference compared to L2 and L3. For L2 and L3, the natural gas production levels are −1488.96 and −2763.38 m^3, respectively (negative values indicate that natural gas input exceeds output when mixed into the injected air).

Compared to natural gas, petroleum typically exhibits lower activation energy for conversion, leading to its earlier formation during the in-situ conversion process (ICP) (Hou et al., 2022). In the field-scale engineering development of autothermal in-situ conversion, the reactions progress sequentially. Hydrocarbons generated in the initial stages are subsequently consumed through secondary cracking reactions (including thermal cracking and hydrocracking) as the process advances. Consequently, significant oil production only commences after approximately two years. This delay corresponds to the period required for the generated liquid hydrocarbons to migrate to the vicinity of the production wells.

This suggests that substantial natural gas oxidation occurs during extraction, with the heat released supplementing the autogenous thermal reaction area. Oil production for L2 and L3 reaches 8.91 and 8.50 m^3, respectively, with L2 producing 4.82% more oil than L3. L2 also achieves peak oil production earlier and has a higher cumulative output compared to L3. Based on the analysis of experimental groups L1, L2, and L3, the significantly lower oil production in Group L1 compared to L2 and L3 is attributed to the injection of 100% air post-reaction initiation. Oxygen in the injected air preferentially triggers vigorous oxidation reactions with organic matter (e.g., kerogen) in oil shales, decomposing liquid hydrocarbons into gaseous hydrocarbon species. This results in reduced oil yields and increased gas generation. Additionally, the inherently low oil saturation in these oil shales further limits initial oil productivity. In contrast, Groups L2 and L3 injected natural gas, which generates additional heat through partial combustion or oxidation reactions. However, in Group L1, the insufficient heat release during the process leads to incomplete conversion of kerogen and prechar in the reservoir, further suppressing oil production. Consequently, the applicability of autothermic pyrolysis in-situ conversion process (ATS) technology in low oil content formations is significantly compromised due to these thermodynamic and kinetic limitations.

3.1.2. Energy efficiency

As shown in Fig. 4, the energy efficiency of L1 shows a modest initial increase, peaking at 0.69 after 0.82 years. For L2, peak energy efficiency reaches 3.70 at 2.54 years, while L3 achieves a peak of 2.65 at 3.34 years. Notably, L2 shows a 39.85% improvement in peak energy efficiency over L3, with a 23.97% reduction in the time required to reach this peak. During the extraction phase, the additional chemical energy introduced by the oxidation of natural gas mixed into the injected air causes a decrease in energy efficiency for L2 and L3 by 1.88 and 1.97 years, respectively, following the end of the preheating period. At 2.32 years for L2 and 2.67 years for L3, the energy efficiency dips below that of L1. However, in the later stages, L2 and L3 demonstrate a significant increase in energy efficiency compared to L1.

3.1.3. Kerogen and prechar content

The distribution of concentration of kerogen in the pore in low oil content oil shale, developed with different natural gas ratios, is shown in Fig. 5(a). At the one-year mark, L1 exhibits a significantly

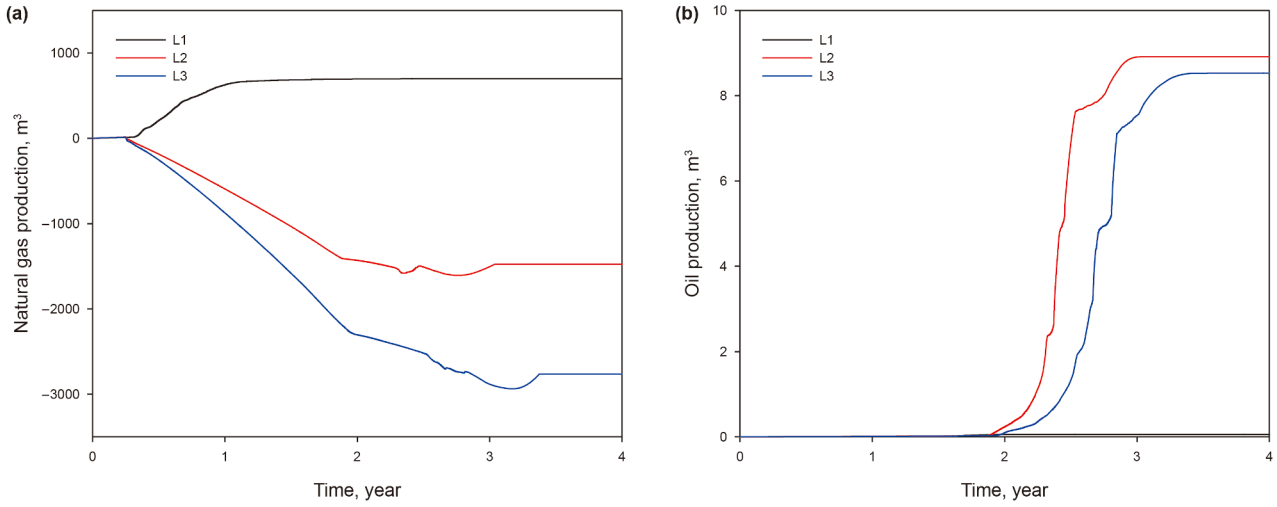

Fig. 3. Relationship between the oil and gas production and time for low oil content shale. (**a**) Natural gas production. (**b**) Oil production.

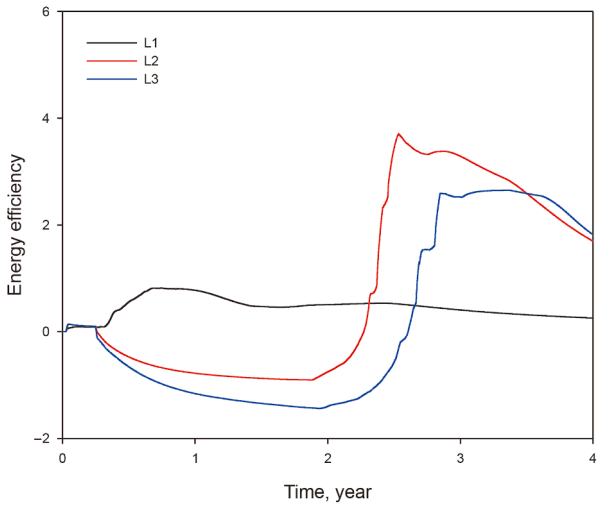

Fig. 4. Relationship between the energy efficiency and time for low oil content shale.

faster kerogen cleavage rate than L2 and L3. By two years, the concentration of kerogen in the pore in L1 approaches that of L2 and L3; however, the pyrolysis reaction in L1 remains less complete compared to L2 and L3. By four years, L1 still shows a small amount of remaining kerogen, whereas L2 and L3 demonstrate similar reaction rates, with thorough kerogen pyrolysis across the formation, completing the reaction within four years. An analysis of prechar distribution within the kerogen layers during extraction (Fig. 5(b)) shows that throughout the L1 reaction, a substantial amount of prechar remains in the formation outside the preheating area. In contrast, L2 and L3 display only minimal prechar distribution at the front end of the reaction zone, with no prechar remaining by the end of the four-year extraction period.

3.1.4. Stratigraphic temperature

The stratigraphic temperature distribution during the development of low oil content oil shale with varying natural gas injection ratios (Fig. 6) shows that the temperatures in L2 and L3 are significantly higher than in L1. The heat generated from the oxidation of the injected natural gas supplements the autogenous thermal reaction zone, resulting in stratigraphic temperatures that exceed those achieved with 100% air injection.

In L1, the temperature in the front stratum drops rapidly between one year and two years. In contrast, the front strata in L2 and L3 maintain higher temperatures during this period. By four years, only a small portion of the L1 formation remains warm, whereas most of the L2 and L3 formations retain higher temperatures. Additionally, comparing L2 and L3 reveals that the central reaction zone in L3 is warmer than in L2 due to the greater oxidative exothermic effect from the higher natural gas injection ratio.

3.1.5. Comparison of options

In terms of oil production, L1 yields significantly less oil compared to L2 and L3, indicating that ATS alone is not effective for low oil content formations. Energy efficiency analysis reveals that both L2 and L3 achieve considerably higher efficiency than L1, with L2 reaching a higher peak efficiency and attaining it earlier than L3. This suggests that there is an optimal level of natural gas in the injected air, rather than simply increasing the gas ratio indefinitely. In this study, the optimal natural gas content is identified as 2.0%.

At the end of extraction, L1 retains a small amount of kerogen and substantial prechar in the formation, whereas L2 and L3 exhibit more complete reactions, with full kerogen pyrolysis and no remaining prechar. Regarding formation temperature, the lower temperatures in L1 do not adequately support kerogen pyrolysis. In contrast, the higher formation temperatures in L2 and L3 facilitate kerogen pyrolysis; however, L3's elevated temperatures—due to the additional oxidative exothermic effect from increased natural gas—accelerate cracking and oil depletion, ultimately reducing oil production. Therefore, L2 maintains a more favorable formation temperature for development.

These findings demonstrate that injecting a small amount of natural gas into low oil content oil shale formations enables effective development where ATS alone would be insufficient. This study on H-ATS for low oil content oil shale indicates that mixing a specific ratio of natural gas into the injected air aids in sustaining the autogenous thermal oxidation reaction. Notably, the natural gas ratio should not be excessively high; an optimal value of 2.0% is recommended based on these results.

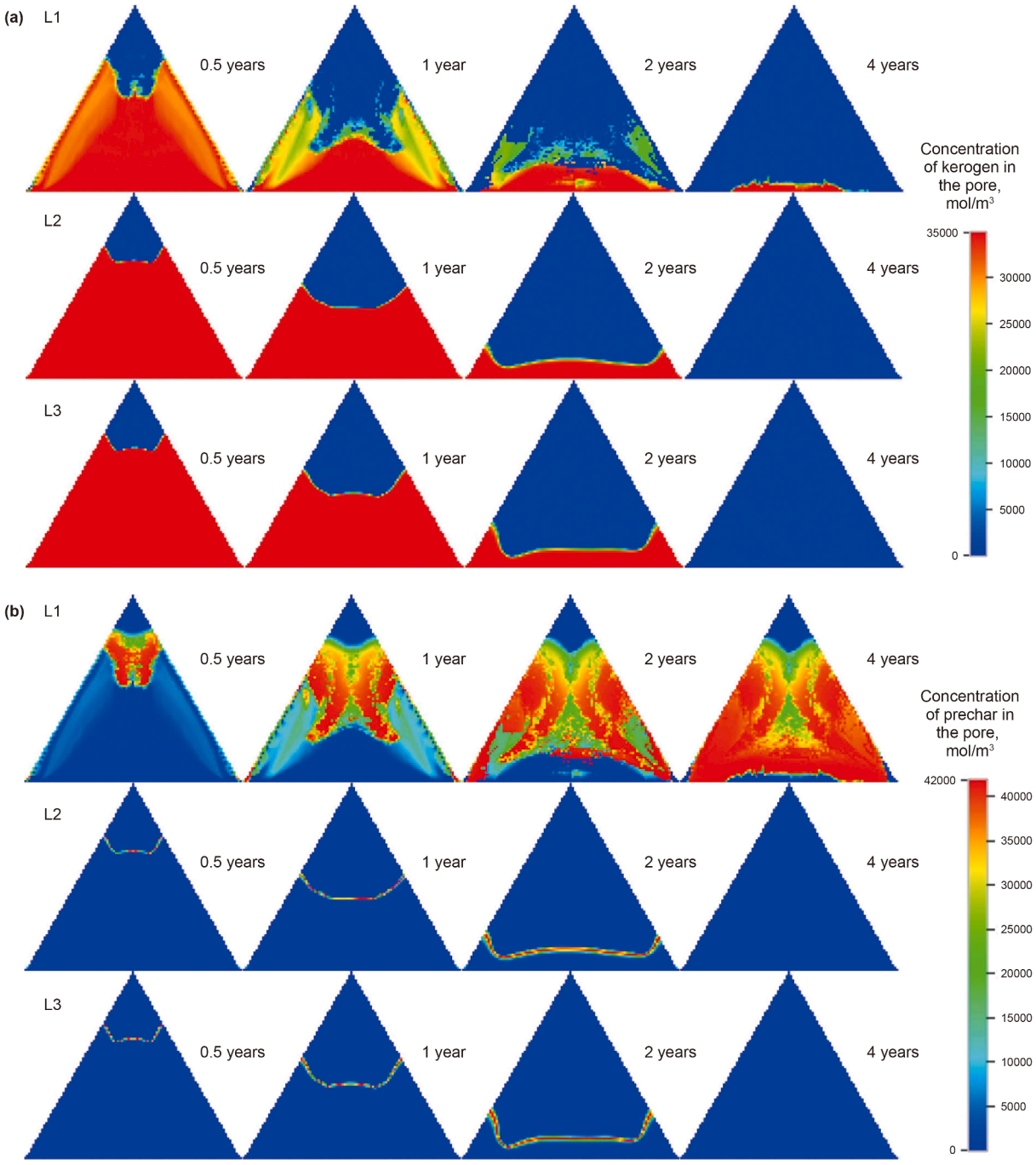

Fig. 5. Kerogen and prechar distribution in the low oil content shale during the H-ATS. (**a**) Kerogen. (**b**) Prechar.

3.2. Medium oil content formation

To study the H-ATS process in medium oil content shale, three different gas injection ratios were applied: 100% air (M1), 98.0% air + 2.0% natural gas (M2), and 96.0% air + 4.0% natural gas (M3). The M1 scenario, with 100% air injection, serves as the baseline model representing conventional autogenous thermal in-situ transformation (ATS) for medium oil content oil shale. This setup allows for an assessment of H-ATS reaction efficiency in medium oil content formations by comparing M1, M2, and M3.

The relationship between oil and gas production over time for medium oil content H-ATS mixtures is shown in Fig. 7. Energy efficiency over time, along with the pore concentration of prechar, is illustrated in Fig. 8. Given that kerogen in low oil content formations is nearly completely reacted by air injection, it is assumed that kerogen in medium and high oil content formations will also undergo complete pyrolysis, so incomplete pyrolysis is not considered. The evolution of oil saturation distribution in the formation is shown in Fig. 9, while Fig. 10 displays the time progression of natural gas injection compression energy, output thermal energy, and output chemical energy. The detailed analysis of these findings is presented below.

3.2.1. Hydrocarbon production

Oil and gas production from the autogenous thermal in-situ extraction of medium oil content oil shale is shown in Fig. 7. The

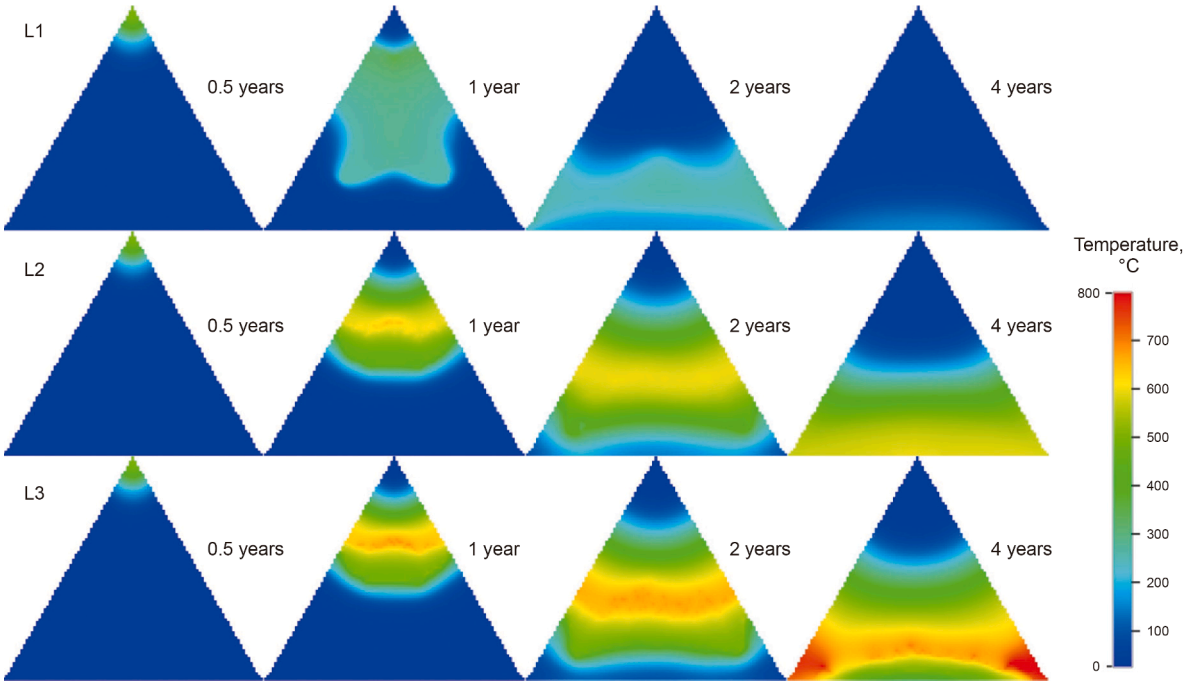

Fig. 6. Temperature distribution in the fracture for low oil content shale.

natural gas production values for M1, M2, and M3 are 1932.31, 407.86, and 255.28 m^3, respectively. Unlike the low oil content formations, where natural gas output is less than the injected volume, all medium oil content formations produce more natural gas than injected. The onset of oil production from medium oil content shale occurs approximately two years after the initiation of autothermic pyrolysis in-situ conversion process, consistent with the production timeline observed in low oil content shale. This temporal pattern arises from the requisite period for hydrocarbon migration to production wells. Oil production for M1, M2, and M3 is 19.09, 17.67, and 13.79 m^3, respectively, at the end of the production periods (3.71 years for M1, 4.09 years for M2, and 4.57 years for M3). M2 shows 7.44% lower oil production and a 10.24% increase in production time compared to M1. Increasing the natural gas proportion further to 4.0% (M3) reduces oil production by 27.76% and extends the production time by 23.18% compared to M1. Overall, hydrocarbon production is inversely correlated with the proportion of natural gas mixed in the injected air.

An analysis of the oil and gas production curves over time (Fig. 7) reveals notable differences between M3 and the other models (M1 and M2). Specifically, M3 displays two distinct phases of natural gas production. Oil production in M3 begins to increase rapidly at approximately 2.15 years, but this rate slows between 2.65 and 4.22 years, followed by a second sharp rise after 4.22 years. These two distinct phases of oil production in M3 are likely due to tampering effects within the formation.

3.2.2. *Energy efficiency*

During the simulation of autogenous thermal in-situ development for medium oil content shale, it is assumed that the kerogen

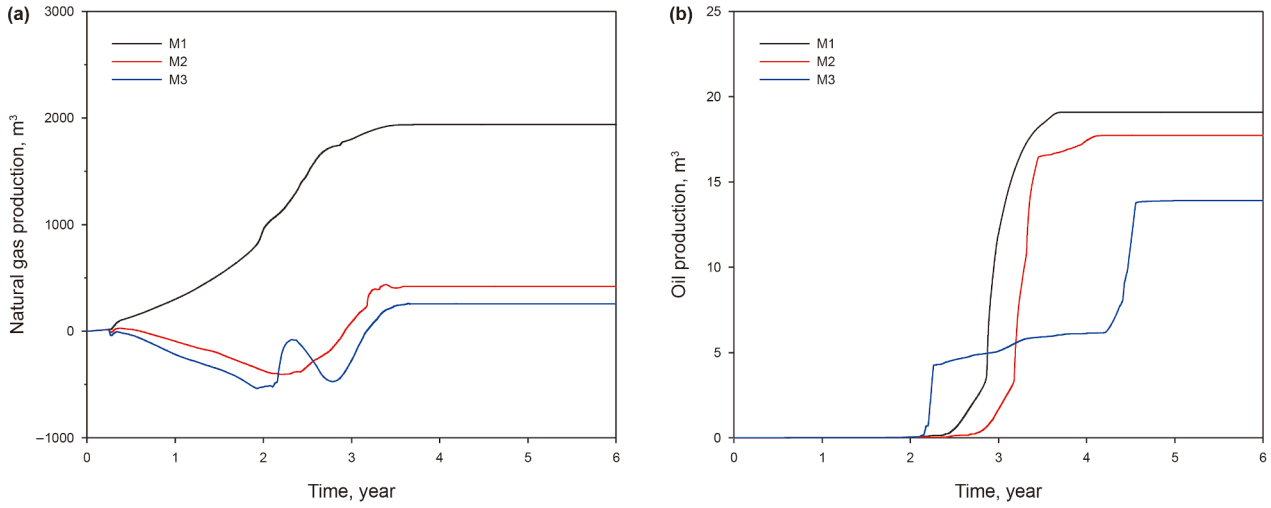

Fig. 7. Relationship between the oil and gas production and time of M1–M3. (**a**) Natural gas production. (**b**) Oil production.

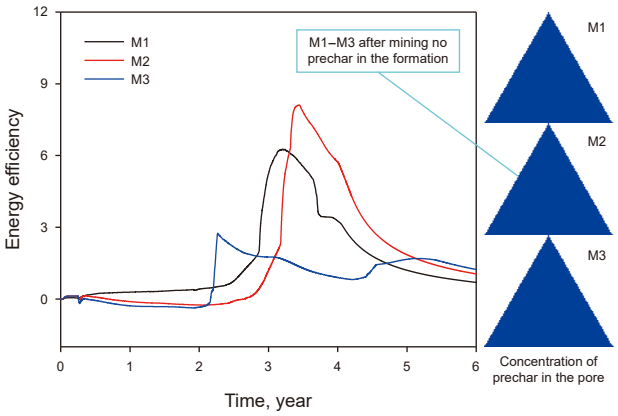

Fig. 8. Relationship between the energy efficiency and time of M1–M3.

reacts fully, resulting in zero semi-coke concentration in the formation at the end of development, indicating full resource utilization. The energy efficiency versus time for H-ATS in medium oil content formations is shown in Fig. 8. M1 and M2 reach their peak energy efficiencies of 6.26 and 8.11 at 3.21 and 3.45 years, respectively. M2 demonstrates a 29.47% increase in peak energy efficiency and a 7.51% increase in time to peak compared to M1. When the natural gas proportion is further increased to 4.0% (M3), peak energy efficiency decreases to 2.73, with a reduced peak time of 2.27 years. Compared to M1, M3 shows a 59.87% decrease in energy efficiency and a 29.40% decrease in peak time. When compared to M2, M3 exhibits a 56.42% lower energy efficiency and a 34.33% shorter time to peak. This decline in M3's energy efficiency and time to peak is attributed to a tampering effect in the formation during development.

M1 reaches a peak energy efficiency of 6.26 at 3.21 years, while M2 achieves a higher peak of 8.11 at 3.45 years, representing a 29.47% increase in energy efficiency and a 7.51% longer time to peak compared to M1 (Fig. 8). In contrast, M3 peaks at 2.73 at 2.27 years, showing a 59.87% reduction in energy efficiency and a 29.40% decrease in time to peak compared to M1. When compared to M2, M3 demonstrates a 56.42% lower energy efficiency and a 34.33% shorter time to peak. Based on the chemical reaction models (as shown in Table 3) established for kerogen and prechar in this study, both kerogen and prechar undergo cracking and oxidation reactions. Under prolonged (>4 years) high-volume injection of air or air mixed with natural gas, the numerical models indicate complete conversion of kerogen and prechar due to the more idealized pore distribution and higher oil saturation in the geological models, which enhances exothermic heat release from oxidation reactions. In contrast, actual field developments exhibit incomplete reactions owing to reservoir heterogeneity, resulting in complete reactions near porous pathways where fluid-rock interactions are vigorous, while regions away from these zones experience incomplete reactions due to restricted mass transfer and heterogeneous permeability distributions.

Analyzing the characteristics of the M3 energy efficiency curve reveals distinct differences from M1 and M2. The energy efficiency in M3 begins to rise rapidly at 2.15 years, earlier than M1 and M2, and features two distinct peaks over the course of the development process. Fig. 8 illustrates this early increase, with M3 exhibiting two phases of rising energy efficiency. The observed decline in M3's energy efficiency and the earlier peak time are attributed to a "flushing" effect occurring within the formation during development, which aligns with the two peaks observed in the oil and gas production curve in Fig. 7.

Natural gas, due to its lower density, tends to migrate rapidly along high-permeability pathways within reservoirs, such as fractures and faults. When the proportion of natural gas in the injected mixture is elevated, it may preferentially accumulate near production wells, inducing heterogeneous reaction distribution and channeling phenomena. In formation with higher oil saturation (>5%), large-scale injection of natural gas can lead to gas aggregation near production wells during the 2-year experimental period, when autogenic thermal reactions reach this region. This results in excessively vigorous reactions, localized overheating

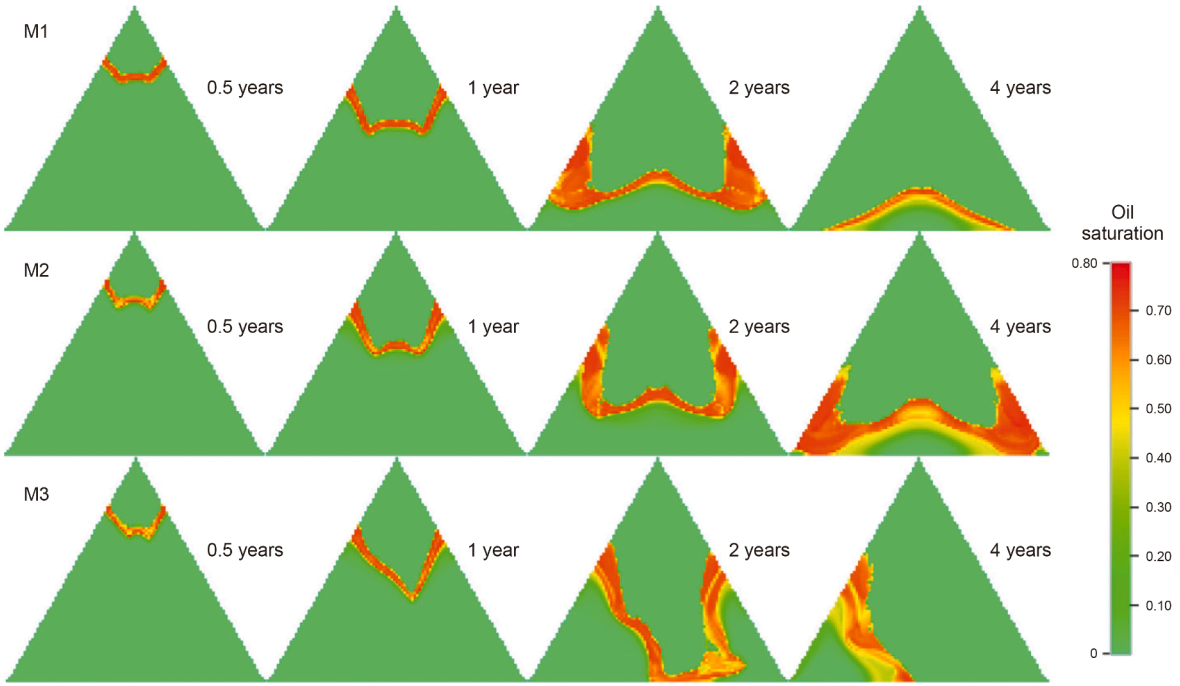

Fig. 9. Oil saturation distribution in the fracture during the M1–M3.

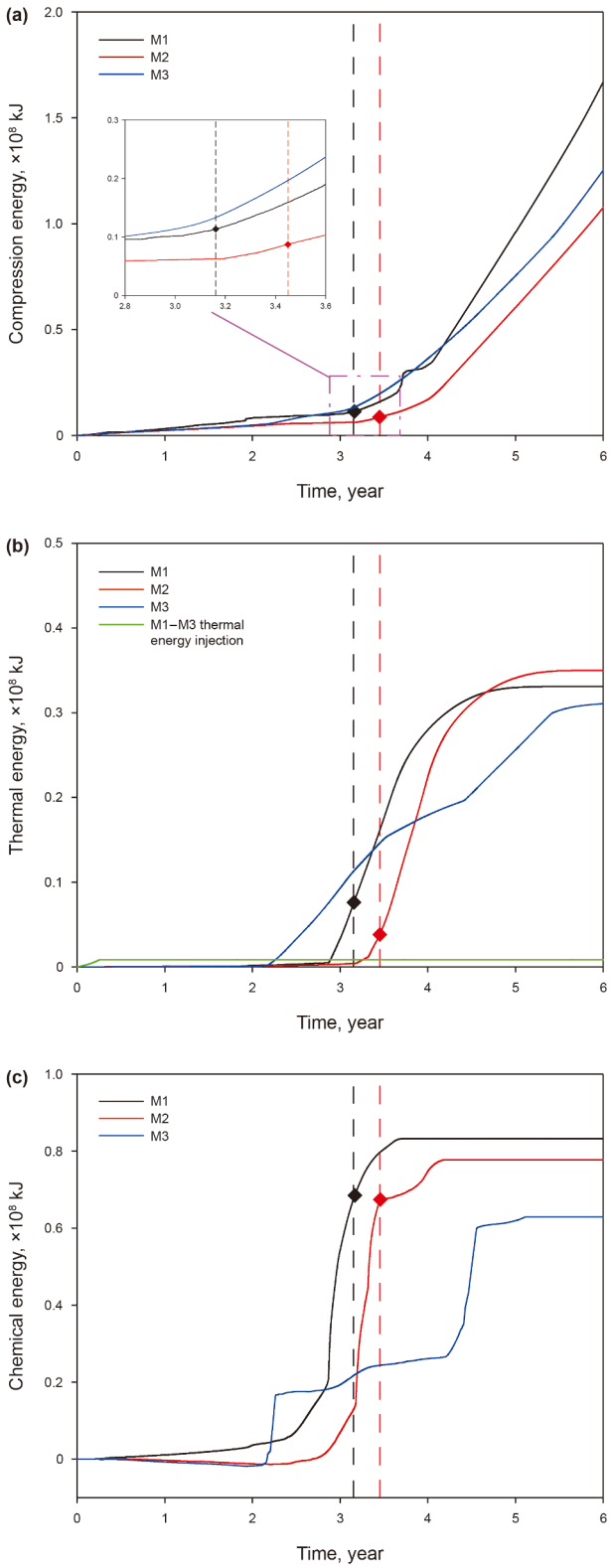

Fig. 10. Relationship between different kinds of energy and time of M1–M3. (**a**) Compression energy. (**b**) Thermal energy production. (**c**) Chemical energy production.

zones, and extensive fracturing near wellbores. Simultaneously, hydrocarbons within the formation experience accelerated escape due to pressure differentials. The oil production rate of M3 exhibited a sharp rise followed by rapid decline at the 2-year mark, as evidenced by oil saturation distribution maps showing faster propagation of oil product fronts toward the right side of the production well. The transient increase in gas production at this stage indicates preferential flow of the gas mixture through fractures, with injected natural gas failing to sustain in-situ pyrolysis reactions. Instead, it migrates through fractures, carrying away thermal energy that could otherwise contribute to hydrocarbon cracking. This inefficient heat utilization, coupled with gas leakage via fractures, directly contributes to reduced energy efficiency by diverting thermal energy away from productive hydrocarbon conversion processes.

3.2.3. Oil saturation

To investigate the distinctive energy efficiency curve of M3 compared to M1 and M2, distribution cloud diagrams of formation oil saturation at key time points were analyzed for each model (Fig. 9). The results indicate that the oil-bearing zones in M1 and M2 advance symmetrically and uniformly within the triangular development area. In M3, however, the oil-bearing zone advances symmetrically only during the early extraction stage. At one year, the oil-bearing zone shifts towards the right, resulting in an asynchronous oil production pattern between the two production wells. Eventually, the two production wells in M3 do not complete oil extraction simultaneously, leading to a substantial accumulation of oil near the left production well. This results in significant oil siltation in certain areas of the formation, while the oil-bearing zone near the right production well depletes, leaving a single gas phase with high gas permeability in the surrounding formation. The disparity in gas permeability between the two production wells causes a flow imbalance, with large volumes of high-pressure gas produced from the right well, reducing its effectiveness in displacing oil. The asynchronous oil production in M3's wells leads to two distinct rises in energy efficiency. The prolonged presence of oil siltation within the formation is the primary factor contributing to the lower overall energy efficiency in M3.

3.2.4. Energy transformation

Although H-ATS reduces the overall oil and gas production, it significantly enhances energy efficiency. This effect is primarily influenced by the transformation of four types of energy during in-situ conversion: injected thermal energy, injected compression energy, produced thermal energy, and produced chemical energy. Investigating these energy transformations helps identify the key factors affecting H-ATS energy efficiency.

As shown in Fig. 10, the changes over time in injected compression energy, produced thermal energy, and produced chemical energy reveal that, despite reducing final oil and gas production, H-ATS significantly boosts energy efficiency through these energy changes. The impact of injected high-temperature nitrogen during the preheating stage is minimal, as the preheating period is short and the formation's permeability remains low during this time. The trends in compression energy from M1 to M3 are generally similar, though M1 has the highest compression energy, followed by M3, with M2 slightly lower than M3. For produced thermal energy, M1 and M2 show similar trends, whereas M3 experiences fluctuations at 3.5 and 4.5 years, likely due to formation flow dynamics. Likewise, chemical energy production in M1 and M2 follows similar trends, with M1 being slightly higher than M2. In contrast, M3 shows a rapid rise in chemical energy in the early stages, with two noticeable fluctuations, which align with the thermal energy fluctuations and are likely related to formation flow effects, possibly a "tampering" phenomenon.

Produced chemical energy rises fastest during the initial extraction phase, acting as the dominant factor in energy

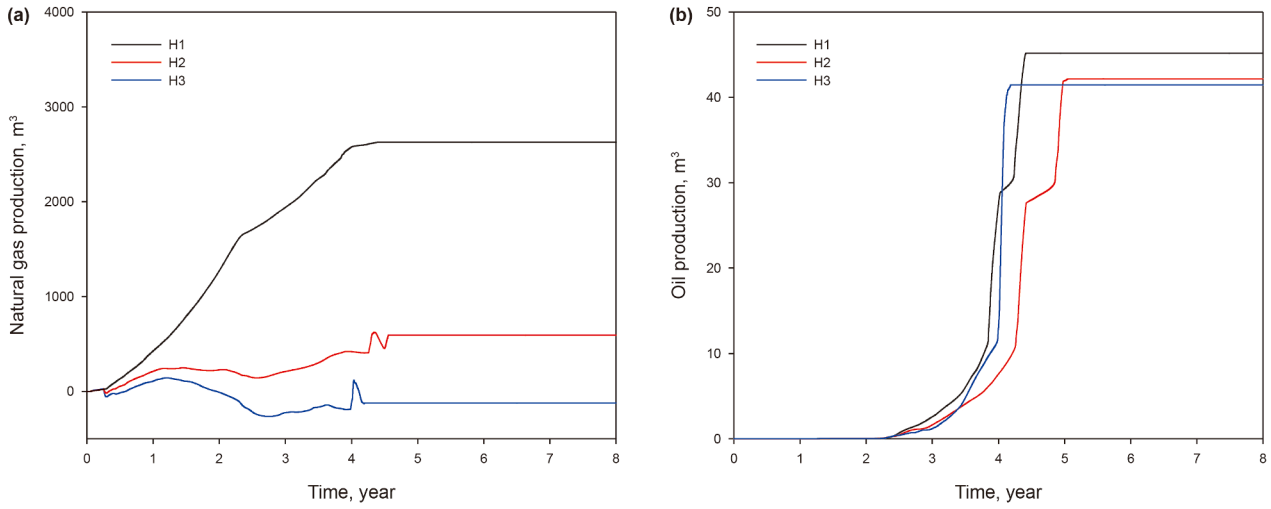

Fig. 11. Relationship between the oil and gas production and time of H1–H3. (**a**) Natural gas production. (**b**) Oil production.

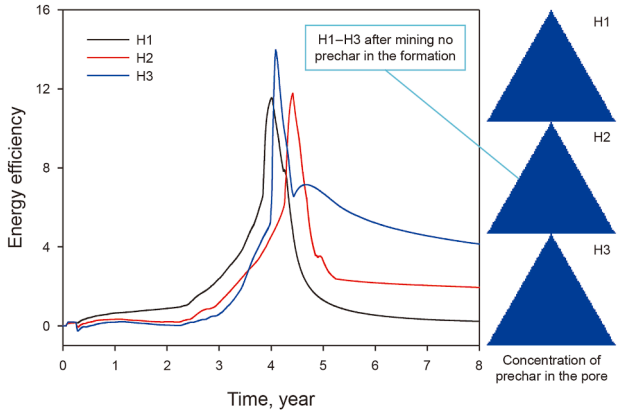

Fig. 12. Relationship between the energy efficiency and time of H1–H3.

efficiency gains. In the later stages, as high-temperature gas production increases, thermal energy also rises. When the reaction zone reaches the production well, formation permeability increases, causing a rapid increase in the high-pressure gas flow rate at the injection well. This, in turn, leads to a sharp rise in compression energy injection, which exceeds the produced chemical and thermal energy, becoming the dominant factor influencing energy efficiency in the final extraction stages.

3.2.5. Comparison of options

The H-ATS study on medium oil content oil shale reveals an inverse correlation between oil and gas production and the proportion of natural gas mixed in the injected air. However, M2 achieves a significantly higher peak energy efficiency than M1, indicating that H-ATS can substantially increase energy efficiency, with an optimal natural gas ratio of 2.0% in this study. Due to flow dynamics in the formation, M3's energy efficiency decreases and reaches its peak earlier, suggesting that the natural gas proportion should remain below 4% for optimal energy efficiency.

While H-ATS results in reduced oil production in the autogenous thermal in-situ conversion of medium oil content oil shale, the decline in production becomes more pronounced with higher natural gas ratios in the injected air. Despite this reduction in final oil and gas output, H-ATS markedly decreases the compression energy needed during the production stage, thereby improving overall energy efficiency. This study concludes that adding a small amount of natural gas to the injected air can effectively support the development of medium oil content formations, with an optimal natural gas content between 0 and 4%, and specifically 2% in this case.

3.3. High oil content formation

To study H-ATS in high oil content shale, three injection scenarios were applied: 100% air (H1), 98.0% air + 2.0% natural gas (H2), and 96.0% air + 4.0% natural gas (H3). The 100% air injection model (H1) serves as a baseline representing conventional autogenous thermal in-situ transformation (ATS) for high oil content formations, allowing for comparison with H2 and H3 to assess the reaction efficiency of H-ATS.

The relationship between oil and gas production over time for H-ATS in high oil content formations is shown in Fig. 11, while Fig. 12 illustrates energy efficiency over time and pore concentration of prechar. Since low oil content formations injected with air show nearly complete kerogen reaction, it is assumed that medium and high oil content formations also undergo complete kerogen pyrolysis, with incomplete pyrolysis being negligible. The evolution of natural gas distribution in the formation is depicted in Fig. 13. Specific analyses of these findings are discussed below.

3.3.1. Hydrocarbons production

Oil and gas production for H-ATS in high oil content formations is shown in Fig. 11. The natural gas production volumes for H1, H2, and H3 are 2617.90, 592.80, and −91.85 m^3, respectively. Analysis of H-ATS natural gas production across low, medium, and high oil content formations indicates a negative correlation between natural gas production and the proportion of mixed natural gas. Similar to medium-to-low oil content shale, the onset of oil production from high oil content shale occurs approximately two years after the initiation of autothermal in-situ conversion (AIC), as the reaction-generated hydrocarbons migrate to production wells. Oil production volumes for H1, H2, and H3 are 45.15, 42.16, and 41.44 m^3, with production periods ending at 4.41, 5.07, and 4.18 years, respectively.

Compared to H1, H2 shows a 6.62% reduction in oil production and a 14.97% increase in production time. Increasing the natural

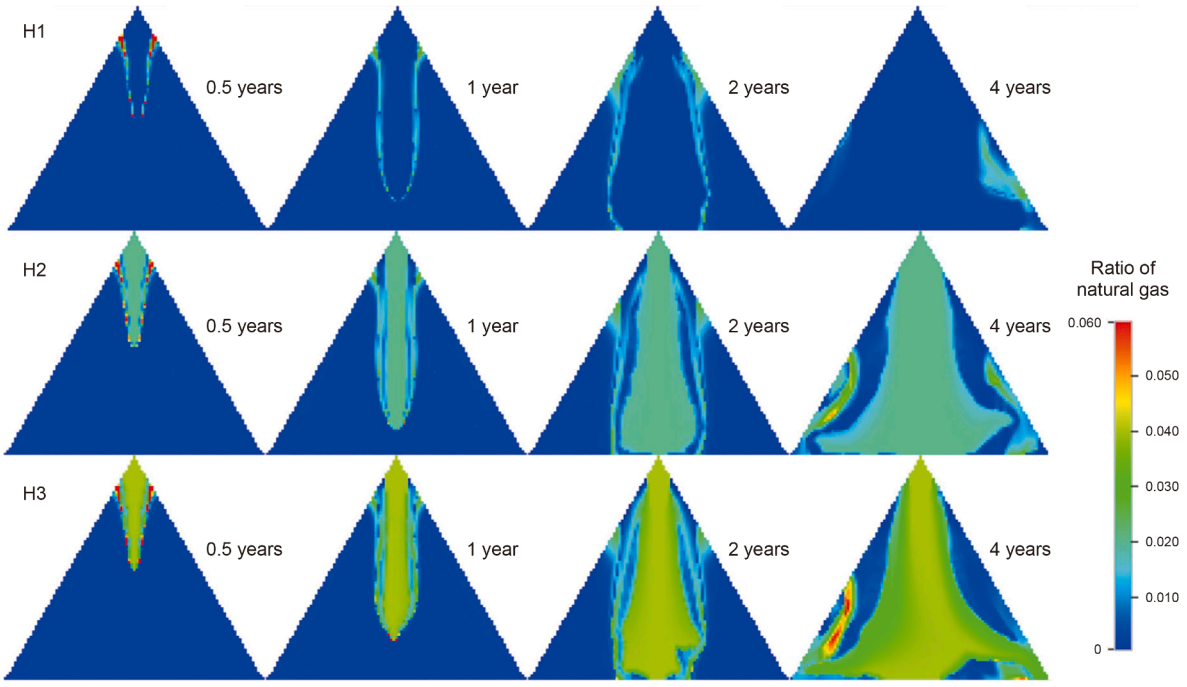

Fig. 13. Ratio of natural gas distribution in the fracture during the H1–H3.

Table 5
ATS oil and gas production and energy efficiency simulation development results.

No.	Oil content, %	Mixed natural gas proportion, %	Oil production, m^3	Gas production, m^3	Energy efficiency
L1	3.0	0	0.06	698.54	0.69
L2	3.0	2.0	8.91	−1476.17	3.70
L3	3.0	4.0	8.53	−2763.38	2.99
M1	5.0	0	19.09	1937.29	6.26
M2	5.0	2.0	17.72	419.83	8.11
M3	5.0	4.0	13.91	255.28	2.74
H1	10.0	0	45.16	2627.26	11.55
H2	10.0	2.0	42.16	592.80	11.77
H3	10.0	4.0	41.47	−122.88	13.97

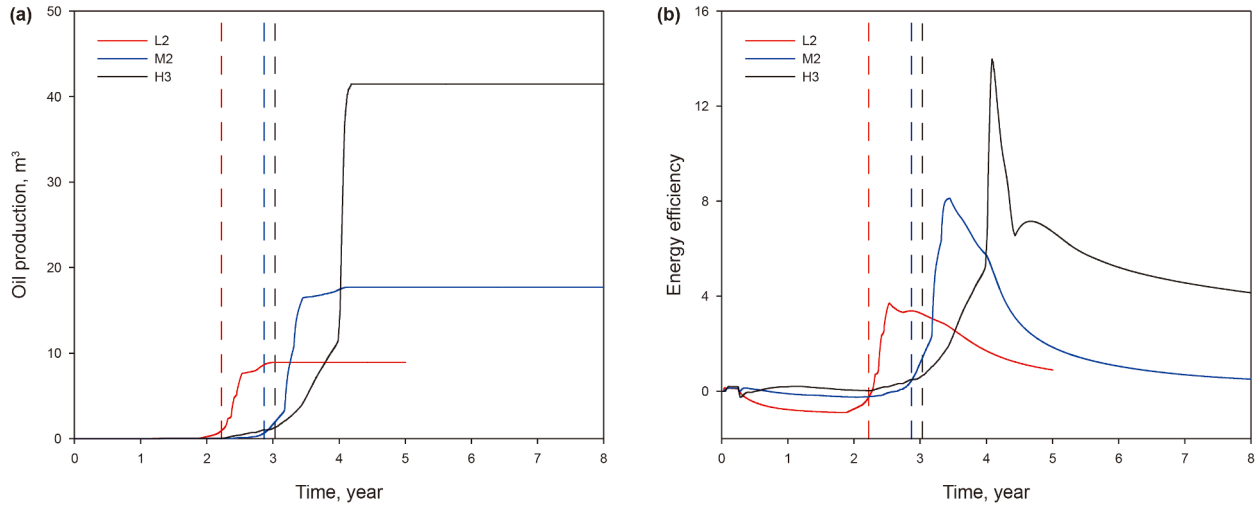

Fig. 14. Relationship between the development effects and time of L2, M2, and H3. (**a**) Oil production. (**b**) Energy efficiency.

gas proportion to 4.0% in H3 results in an 8.22% decrease in oil production and a 5.22% reduction in production time compared to H1, indicating a negative correlation between oil production and the proportion of natural gas in the injected mix.

3.3.2. Energy efficiency

As shown in Fig. 12, based on the analysis of kerogen and prechar in moderately oil-saturated formations, prolonged injection of air or air-natural gas mixtures in higher oil-saturated reservoirs leads to complete conversion of kerogen and prechar through cracking and oxidation processes. However, in actual field-scale developments, reservoir heterogeneity results in incomplete cracking and oxidation reactions due to spatial variations in porosity and permeability distributions. The peak energy efficiency for H1 is 11.67, reached at 4.01 years; for H2, the peak is 11.77, reached at 4.42 years; and for H3, the peak is 13.91, reached at 4.09 years. Compared to H1, H2 shows a 0.86% increase in peak energy efficiency and a 10.14% longer time to reach this peak. H3, on the other hand, increases energy efficiency by 19.19% and reduces the time to reach peak efficiency by 1.92% compared to H1. Both H2 and H3 enhance the energy efficiency of the conventional ATS process for high oil content formations, with H-ATS proving superior across low, medium, and high oil content formations. Specifically, H3 demonstrates an 18.18% increase in energy efficiency and a 7.46% reduction in time to peak efficiency compared to H2, indicating that a 4.0% natural gas ratio is optimal for H-ATS in high oil content formations.

3.3.3. Ratio of hydrocarbon gases

While oil production and energy efficiency in H-ATS for high oil content formations show no clear trend or significant divergence, natural gas production does exhibit noticeable fluctuations. Using the proportion of natural gas within the formation gas as an indicator, the distribution of natural gas at key time points for H1 to H3 is illustrated in Fig. 13. This analysis shows that in H1, natural gas is primarily concentrated in a small area at the reaction front, whereas in H2 and H3, natural gas concentrations are higher across the entire reaction area. Notably, H3 has a significantly higher natural gas concentration than H2, indicating that natural gas in H3 is more readily oxidized and consumed. Consequently, during H-ATS development, injecting mixed natural gas increases the concentration of natural gas in the formation, leading to its oxidation and consumption. This process reduces natural gas production and, in turn, decreases total oil and gas output.

3.4. Comparison of the development effect of different oil content

A comprehensive comparison of in-situ development across nine oil shale formations with varying H-ATS ratios for low, medium, and high oil content (Table 5) indicates that incorporating a certain proportion of natural gas in H-ATS improves energy efficiency in formations of different oil content, with the most pronounced effect observed in low oil content formations. Generally, natural gas production negatively correlates with the proportion of blended natural gas across formations with different oil content levels. For low oil content formations, where ATS alone is ineffective, oil production remains minimal. In medium and high oil content formations, oil production also shows a negative correlation with the proportion of blended natural gas.

The comparison reveals that an H-ATS mixture with 2% natural gas yields optimal results for low (L2) and medium (M2) oil content formations, while 4% natural gas (H3) is most effective for high oil content formations. Gas production in high oil content formations is notably lower than in medium oil content formations due to higher natural gas concentration within the formation, leading to greater oxidation and consumption of natural gas. Across all formations, higher proportions of mixed natural gas in H-ATS consistently result in significantly reduced gas production, with only a slight decrease in oil production.

The optimal H-ATS development groups for low, medium, and high oil content formations, i.e., L2, M2, and H3, were compared based on energy efficiency and oil production (Fig. 14). The times for the onset of rapid oil production in L2, M2, and H3 were 2.22, 2.87, and 3.03 years, respectively. Compared to L2, the onset of rapid oil production was delayed by 28.96% in M2 and by 36.34% in H3. These results indicate that the initial rise in the slope of the energy efficiency curve coincides with the beginning of the rise in oil production, and the period of rapid increase in energy efficiency aligns with the period of accelerated oil production. Furthermore, the time to reach rapid oil production correlates positively with the formation's oil content. It suggests that as oil production begins to rise sharply, energy efficiency follows suit, while a decrease in oil production similarly reflects a decline in energy efficiency. This highlights the utility of energy efficiency as an index for evaluating extraction performance in real-world production.

The variation in the onset of rapid increases in energy efficiency and oil production across the three groups is attributed to two primary factors: first, the heat required for cracking increases with the formation's kerogen concentration, and second, higher oil content formations produce more oil upon cracking, extending the time for oil and gas migration to production wells. The difference in peak oil production and energy efficiency among the three groups corresponds to oil content, with higher oil content formations achieving higher oil production and energy efficiency. Consequently, the differences in curve characteristics reflect only the oil content variations in the formations. From an energy efficiency perspective, the energy efficiency curves of the three optimal models exhibit consistent trends, demonstrating that H-ATS enhances energy efficiency uniformly across formations with varying oil content, thereby supporting its effectiveness in developing formations of different oil contents.

The heat generated from the oxidation of organic components in low oil content formations (2.9% oil content) is insufficient to sustain continuous autogenous heat generation, making the addition of a certain proportion of natural gas essential for successful ATS. In medium and high oil content formations, natural gas mixing is not strictly required for ATS success. However, incorporating an optimal amount of natural gas can significantly improve energy efficiency. Notably, increasing the proportion of natural gas does not indefinitely enhance results, and there exists an optimal proportion that depends on the formation's oil content.

4. Conclusions

This study investigates the effects of H-ATS on oil shale formations with varying oil content through numerical simulations. By analyzing oil and gas production, energy efficiency, formation temperature, and physical evolution, the influence of natural gas assistance on the autogenous thermal in-situ conversion of oil shale is examined, and the applicability of H-ATS for formations with different oil contents is clarified. The main conclusions are as follows.

(1) Low oil content formations: For low oil content oil shale, conventional ATS using air injection is insufficient due to the limited heat generated from organic matter oxidation. However, the addition of a small amount of natural gas aids the in-situ conversion by enhancing autogenous heat generation, achieving an energy efficiency of up to 3.70. The optimal natural gas ratio is around 2.0%, as a higher

concentration reduces energy efficiency and prolongs development time. Therefore, H-ATS is recommended for low oil content formations, as it significantly enhances energy efficiency and oil production by sustaining the autogenous thermal oxidation reaction.

(2) Medium oil content formations: In medium oil content formations, H-ATS notably reduces the required compression energy during the production phase, thus increasing overall energy efficiency. For formations with 5.0% oil content, a 2.0% natural gas blend achieves a peak energy efficiency of 8.11%–29.47% higher than with air alone—while decreasing oil production by only 7.44% compared to conventional ATS. This suggests that blending a small amount of natural gas in medium oil content formations can improve energy efficiency with minimal impact on oil production. In this study, 2.0% is identified as the optimal natural gas proportion for medium oil content formations.

(3) High oil content formations: Similar to medium oil content formations, H-ATS in high oil content formations enhances energy efficiency by reducing compression energy input. For formations with 9.8% oil content and a 4.0% natural gas blend, energy efficiency reaches 13.04%–19.19% higher than with air alone—though oil production is 8.22% lower than with conventional ATS. While H-ATS improves energy efficiency in high oil content formations, economic considerations may favor conventional ATS, which offers higher oil and gas production with better cost-effectiveness. For high oil content formations, ATS remains preferable, but a small proportion of natural gas can still provide a boost in energy efficiency.

CRediT authorship contribution statement

Chao-Fan Zhu: Writing – original draft, Supervision, Software, Methodology, Investigation, Conceptualization. **Tan-En Jiang:** Writing – review & editing, Writing – original draft, Software. **Shan-Shan Yao:** Writing – review & editing, Visualization. **Jia-Zong Li:** Validation, Methodology. **Rui Jia:** Supervision, Formal analysis. **Wei Guo:** Supervision, Resources, Funding acquisition, Conceptualization.

Declaration of competing interest

The authors declare that they have no known competing financial interests or personal relationships that could have appeared to influence the work reported in this paper.

Acknowledgments

This work is supported by the Key R&D Projects of Jilin Provincial Science and Technology Department (Grant No. 20230203121SF) and the Open Fund Project of State Energy Shale Oil Research and Development Center (Grant No. 33550000-24-ZC0613-0055).

References

Bai, W.X., Sun, Y.H., Guo, W., et al., 2017. Pilot test project of oil shale in-situ pyrolysis in Nong'an of Jilin. In: Proceedings of the 19th National Academic Exchange Conference on Prospecting Engineering (Geotechnical Drilling and Excavation Engineering). Urumqi, Xinjiang, China (in Chinese).

Bauman, J.H., Huang, C.K., Gani, M.R., et al., 2009. Modeling of the in-situ production of oil from oil shale. Oil Shale: A Solution to the Liquid Fuel Diemma. 135–146. https://doi.org/10.1021/bk-2010-1032.ch007.

Braun, R.L., Burnham, A.K., 1992. PMOD: A flexible model of oil and gas generation, cracking, and expulsion. Org. Geochem. (1), 161–172. https://doi.org/10.1016/0146-6380(92)90034-U.

Dong, F.K., Feng, Z.J., Yang, D., et al., 2018. Permeability evolution of pyrolytically-fractured oil shale under in situ conditions. Energies 11, 3033. https://doi.org/10.3390/en11113033.

Dyni, J.R., 2003. Geology and resources of some world oil-shale deposits. Oil Shale 20 (3), 193–252. https://doi.org/10.3133/sir29955294.

Fan, D.J., 2022. Research on Paleoclimate, Paleoenvironment and Source Rock Development Model of the Cretaceous Shahezi Formation in Xujiaweizi Fault Depression, Songliao Basin. PhD Dissertation. Jilin Universtiy. https://doi.org/10.27162/d.cnki.gjlin.2022.007506.

Fan, Y., Durlofsky, L.J., 2010. Tchelepi H.A. numerical simulation of the in-situ upgrading of oil shale. SPE J. 15 (2), 368–381. https://doi.org/10.2118/118958-PA.

Fowler, T.D., Vinegar, H.J., 2009. Oil shale ICP-colorado field pilots. SPE Western Regional Meeting. https://doi.org/10.2118/121164-MS.

Guo, H.F., Cheng, Q.X., Wang, D., et al., 2016. Analyzing the contribution of semicokes to forming self-heating in the oil-shale self-heating retorting process. Energy Fuels 30 (7), 5355–5362. https://doi.org/10.1021/acs.energyfuels.6b00351.

Guo, W., Yang, Q.C., Sun, Y.H., et al., 2020. Characteristics of low temperature co-current oxidizing pyrolysis of Huadian oil shale. J. Anal. Appl. Pyrolysis 146, 104759. https://doi.org/10.1016/j.jaap.2019.104759.

Guo, W., Yang, Q., Deng, S., et al., 2022. Experimental study of the autothermic pyrolysis in-situ conversion process (ATS) for oil shale recovery. Energy 258, 124878. https://doi.org/10.1016/j.energy.2022.124878.

Guo, W., Li, Q., Deng, S.H., et al., 2023a. Mechanism and reservoir simulation study of the autothermic pyrolysis in-situ conversion process for oil shale recovery. Pet. Sci. 20 (2), 1053–1067. https://doi.org/10.1016/j.petsci.2022.08.030.

Guo, W., Zhang, X., Sun, Y.H., et al., 2023b. Migration mechanism of pyrolysis oil during oil shale in situ pyrolysis exploitation. Energy 285, 128769. https://doi.org/10.1016/j.energy.2023.128769.

He, K., Wang, X., Yang, C., et al., 2025. C/H isotope fractionation of hydrocarbon gases from hydrogenation of organic matter: Insights from hydrothermal experiments. Org. Geochem. 199, 104884. https://doi.org/10.1016/j.orggeochem.2024.104884.

He, W.T., Sun, Y.H., Guo, W., et al., 2019. Organic geochemical characteristics of the upper Cretaceous Qingshankou Formation oil shales in the Fuyu Oilfield, Songliao Basin, China: Implications for oil-generation potential and depositional environment. Energies 12 (24), 4778. https://doi.org/10.3390/en12244778.

He, W.T., Sun, Y.H., Shan, X.L., 2021. Organic matter evolution in pyrolysis experiments of oil shale under high pressure: Guidance for in situ conversion of oil shale in the Songliao Basin. J. Anal. Appl. Pyrolysis 155, 105091. https://doi.org/10.1016/j.jaap.2021.105091.

Hou, L., He, K., Zhai, J., et al., 2022. Compositional kinetics for hydrocarbon evolution in the pyrolysis of the Chang 7 organic matter: Implications for in-situ conversion of oil shale. J. Anal. Appl. Pyrolysis 162, 105434. https://doi.org/10.1016/j.jaap.2022.105434.

Kang, Z.Q., Zhao, Y.S., Yang, D., 2020. Review of oil shale in-situ conversion technology. Appl. Energy 269, 115121. https://doi.org/10.1016/j.apenergy.2020.115121.

Khakimova, L., Bondarenko, T., Cheremisin, A., et al., 2019. High pressure air injection kinetic model for Bazhenov Shale Formation based on a set of oxidation studies. J. Petrol. Sci. Eng. 172, 1120–1132. https://doi.org/10.1016/j.petrol.2018.09.021.

Lee, K., Moridis, G.J., Ehlig-Economides, C.A., 2016. A comprehensive simulation model of kerogen pyrolysis for the in-situ upgrading of oil shales. SPE J. 21 (5), 1612–1630. https://doi.org/10.2118/173299-PA.

Lee, K.J., Finsterle, S., Moridis, G.J., 2018. Analyzing the impact of reaction models on the production of hydrocarbons from thermally upgraded oil shales. J. Petrol. Sci. Eng. 168, 448–464. https://doi.org/10.1016/j.petrol.2018.05.021.

Lewan, M.D., 1997. Experiments on the role of water in petroleum formation. Geochem. Cosmochim. Acta 61 (17), 3691–3723. https://doi.org/10.1016/S0016-7037(97)00176-2.

Li, J.Q., Cai, J.C., 2023. Quantitative characterization of fluid occurrence in shale reservoirs. Advances in Geo-Energy Research 9 (3), 146–151. https://doi.org/10.46690/ager.2023.09.02.

Li, Y., Nie, F.J., Yan, Z.B., et al., 2022. Geochemical characteristics and petrogenetic significance of the sandstones of the Sifangtai Formation in Yi'an Area, Northern Songliao Basin. Sci. Technol. Eng. 22 (5), 1814–1820. https://doi.org/10.3969/j.issn.1671-1815.2022.05.011 (in Chinese).

Liang, W.G., Zhao, Y.S., Liu, J.S., et al., 2021. Advances in in-situ modified mining by fluidization and in unconventional geomechanics. Advances in Geo-Energy Research 5 (1), 1–4. https://doi.org/10.46690/ager.2021.01.01.

Pei, S.F., Wang, Y.Y., Zhang, L., et al., 2018. An innovative nitrogen injection assisted in-situ conversion process for oil shale recovery: Mechanism and reservoir simulation study. J. Petrol. Sci. Eng. 171, 507–515. https://doi.org/10.1016/j.petrol.2018.07.071.

Shakib, J.T., Akhgarian, E., Ghaderi, A., 2015. The effect of hydraulic fracture characteristics on production rate in thermal EOR methods. Fuel 141, 226–235. https://doi.org/10.1016/j.fuel.2014.10.063.

Shen, C.H., 2009. Reservoir simulation study of an in-situ conversion pilot of Green-River oil shale. In: SPE Rocky Mountain Petroleum Technology Conference. https://doi.org/10.2118/123142-ms.

Sun, W.G., Liu, X.S., Zhan, T.Y., et al., 2022. Quality characteristics of oil shale of the 1st member of Upper Cretaceous Qingshankou Formation of well JFD3 in southeastern rising area of Songliao Basin. Jilin Geol. 41 (2), 18–23. https://doi.org/10.3969/j.issn.1001-2427.2022.02.003.

Sun, Y., Jin, B.S., Wu, W., et al., 2015a. Effects of temperature and composite alumina on pyrolysis of sewage sludge. J. Environ. Sci. 30, 1–8. https://doi.org/10.1016/j.jes.2014.10.010.

Sun, Y.H., Bai, F.T., Lü, X.S., et al., 2015b. Kinetic study of Huadian oil shale combustion using a multi-stage parallel reaction model. Energy 82, 705–713. https://doi.org/10.1016/j.energy.2015.01.080.

Sun, Y.H., Guo, W., Deng, S.H., 2021. The status and development trend of in-situ conversion and drilling exploitation technology for oil shale. Drilling Engineering 48 (1), 57–67. https://doi.org/10.12143/j.ztgc.2021.01.008 (in Chinese).

Tong, J.H., Han, X.G., Wang, S., et al., 2011. Evaluation of structural characteristics of Huadian oil shale Kerogen using direct techniques (Solid-State ^{13}C NMR, XPS, FT-IR, and XRD). Energy Fuels 25 (9), 4006–4013. https://doi.org/10.1021/ef200738p.

Wang, G.Y., Yang, D., Zhao, Y.S., et al., 2019. Experimental investigation on anisotropic permeability and its relationship with anisotropic thermal cracking of oil shale under high temperature and triaxial stress. Appl. Therm. Eng. 146, 718–725. https://doi.org/10.1016/j.applthermaleng.2018.10.005.

Wang, L., Yang, D., Li, X., et al., 2018a. Macro and meso characteristics of in-situ oil shale pyrolysis using superheated steam. Energies 11 (9), 2297. https://doi.org/10.3390/en11092297.

Wang, L., Yang, D., Zhao, Y.S., et al., 2020. Evolution of pore characteristics in oil shale during pyrolysis under convection and conduction heating modes. Oil Shale 37 (3), 224–241. https://doi.org/10.3176/oil.2020.3.04.

Wang, L., Yang, D., Kang, Z.Q., et al., 2022. Experimental study on the effects of steam temperature on the pore-fracture evolution of oil shale exposed to the convection heating. J. Anal. Appl. Pyrolysis 164, 105533. https://doi.org/10.1016/j.jaap.2022.105533.

Wang, W.M., 2013. Establishment and Application of Evaluation Criteriaof Shale Oil and Gas Resources Potential : a Case of Southern Songliao Basin. Phd Dissertation. Northeast. Petroleum University (in Chinese).

Wang, Y.Y., Ren, S.R., Zhang, L., et al., 2018b. Numerical study of air assisted cyclic steam stimulation process for heavy oil reservoirs: Recovery performance and energy efficiency analysis. Fuel 211, 471–483. https://doi.org/10.1016/j.fuel.2017.09.079.

Xia, Y.L., Zheng, J.W., Li, Z.Y., et al., 2010. Mineralisation characteristics and mineralisation pattern of the Qianjadian uranium deposit, Songliao Basin, China. Miner. Depos. 29 (S1), 154–155. https://doi.org/10.16111/j.0258-7106.2010.s1.087 (in Chinese).

Xu, S.T., 2023. Theoretical and experimental study on thermal initiation process of autothermic pyrolysis in-situ conversion technology for oil shale. PhD dissertation. Jilin University. 21-23. https://link.cnki.net/doi/10.27162/d.cnki.gjlin.2023.000114 (in Chinese).

Yang, F., Cheng, X.Q., Li, M.J., et al., 2023a. Numerical investigation of the heat and mass transfer during the in situ pyrolysis process of oil-rich coal. Processes 11 (11), 3226. https://doi.org/10.3390/pr11113226.

Yang, Q.C., Guo, W., Xu, S.T., et al., 2023b. The autothermic pyrolysis in-situ conversion process for oil shale recovery: Effect of gas injection parameters. Energy 283, 129134. https://doi.org/10.1016/j.energy.2023.129134.

Zhang, L.W., Chen, L., Hu, R., et al., 2022. Subsurface multiphase reactive flow in geologic CO_2 storage: Key impact factors and characterization approaches. Advances in Geo-Energy Research 6 (3), 179–180. https://doi.org/10.46690/ager.2022.03.01.

Zhao, W.Z., Hu, S.Y., Hou, L.H., 2018. Connotation and strategic role of in-situ conversion processing of shale oil underground in the onshore China. Petrol. Explor. Dev. 45 (4), 563–572. https://doi.org/10.1016/S1876-3804(18)30063-6.

Zhao, W.Z., Bian, C.S., Li, Y.X., et al., 2023. Enrichment factors of movable hydrocarbons in lacustrine shale oil and exploration potential of shale oil in Gulong Sag, Songliao Basin, NE China. Petrol. Explor. Dev. 50 (3), 520–533. https://doi.org/10.1016/S1876-3804(23)60407-0.

Zhu, C., Guo, W., Sun, Y., et al., 2022. Reaction mechanism and reservoir simulation study of the high-temperature nitrogen injection in-situ oil shale process: A case study in Songliao Basin, China. Fuel 316, 123164. https://doi.org/10.1016/j.fuel.2022.123164.